

# Revealing Unintentional Information Leakage in Low-Dimensional Facial Portrait Representations

Kathleen Anderson and Thomas Martinetz

Institute for Neuro- and Bioinformatics, University of Lübeck, Germany  
{k.anderson,thomas.martinetz}@uni-luebeck.de

**Abstract.** We evaluate the information that can unintentionally leak into the low dimensional output of a neural network, by reconstructing an input image from a 40- or 32-element feature vector that intends to only describe abstract attributes of a facial portrait. The reconstruction uses blackbox-access to the image encoder which generates the feature vector. Other than previous work, we leverage recent knowledge about image generation and facial similarity, implementing a method that outperforms the current state-of-the-art. Our strategy uses a pre-trained StyleGAN and a new loss function that compares the perceptual similarity of portraits by mapping them into the latent space of a FaceNet embedding. Additionally, we present a new technique that fuses the output of an ensemble, to deliberately generate specific aspects of the recreated image.

**Keywords:** feature vector reconstruction · face recognition · privacy.

Despite the increasing ubiquity of AI solutions, the relevance of privacy in the context of machine learning is often overlooked. One important question is of how much unwanted information can leak into an attribute feature vector. Neural networks are applied to extract, e.g., the stress level of drivers [15], the engagement of students [3,37], a medical diagnosis [13] and abstract avatars<sup>1</sup> from photos of users. They are even proposed for explicitly anonymizing private data [24,39,38,28,29,6,35,27,2,26]. By most of these examples, it is neglected that the information processing of neural networks is not well enough understood to be able to guarantee the absence of private input information in their output. Information that is supposed to be removed could still be a part of the feature vector, only in an altered way.

This paper aims to raise awareness for the fact that we are currently unable to prevent private input information from leaking into the output of a neural network. We reconstruct an input image from a feature vector which should only describe a few attributes of the image, by training a *decoder* (depicted in Figure 1) which reverts from a feature vector back to the input that created it, focusing on recreating components of the input that should not be a part of the feature

<sup>1</sup> One example is the *Bitmoji* created by the *Snapchat* app, see <https://www.bitmoji.com/>

vector. The focus of this paper is set on reconstructing human portraits, with the main target on their identity.

To achieve such a reconstruction, several challenges need to be overcome by the decoder. One is the nature of the mapping from image to feature vector: the relation is not bijective, more than one input can lead to the same output. To counter this problem, we leverage a pretrained StyleGAN [20] image generator to introduce a strong bias towards a defined target distribution. Another difficulty arises from the fact that the exact target of our reconstruction can be hard to define. An optimal decoder would recreate every pixel of the input, which is a complex task, even given our limited search space. This is, however, not necessary: a reconstruction that only incorporates the important parts of the input can be just as harmful (for example a photo of a person with the same identity, taken from a different angle with a different facial expression or background). Hence, optimizing only the pixel-wise error is not a clever approach, and might even favor the reconstruction of the wrong person in front of the right background. Instead, we map both input and reconstructed images into different latent spaces and compare their embeddings.

The combination of various specialized loss functions improves the reconstruction, but also introduces a third challenge: how to blend the result of decoders trained for different goals? We found that combining the losses into a single cost function oftentimes keeps the model from converging - even though all are theoretically aiming for the same perfect solution (an exact reconstruction). A reason might be that the paths of the cost functions during learning are too dissimilar. A solution presented in this paper is to make use of a special property of the StyleGAN image generator: each layer of the image generator creates a certain aspect of the image, like the shape of the face or the pose of the depicted person. By feeding specialized inputs to the individual StyleGAN layers, we can systematically define each component of the generated image.

By explicitly leveraging the different layers of a pretrained StyleGAN, to join the output of an ensemble trained for different specialized loss functions, we are the first to generate truly recognizable reconstructions of input images from attribute vectors. We further demonstrate that a sophisticated training method can be more valuable than a large network architecture: the components of our decoder ensemble are nothing but shallow multi layer perceptrons.

## 1 Related Work

There are many angles from which machine learning models can be attacked. The topic of this paper falls into the category of data reconstruction at inference time. This line of research can be split according to three properties:

- the **knowledge of the attacker**, who is either given access to all model parameters (whitebox) or only allowed to pose queries to the model and receive an answer, with no information about how that answer was calculated (blackbox),

- the **goal of the attack**: either to infer knowledge about the data used to train a model or to reconstruct a specific input, given an output, with the input not having been part of the training set,
- and the **type of encoder**: an encoder trained to extract features from a given image of a person without aiming at being able to reveal the person’s identity or a facial embedding network with features explicitly created to encode the identity of a depicted person.

In the following, we pay particular attention to the two different attack goals. The two goals are similar enough to motivate coinciding strategies but are confronted with different limitations. To the best of our knowledge, the recreation of training data as an attack goal has only been done for encoders that classify whole identities - one class corresponding to exactly one individual. The challenge has been tackled from a whitebox [32,14,41,4] and blackbox [19,7,17] access, sometimes making a similar use of image generators as our method.

The most popular targets for the second goal, a feature vector reconstruction attack, are face embeddings: high-level representations of a face or identity. Again, by design, face embedding networks are trained to condense as much identity information as possible into the embedding vector. [5], for example, even use the reconstruction capability as a quality measure for the embedding. Many blackbox attacks [34,9,22,31,22,8,12] expand upon this goal, proving that if an encoder network is trained to create a condensed version of an identity, this version can be decompressed to reveal most of the original input. By now, major companies<sup>2</sup> have started to recognize this fact and carry out measures to protect such embeddings.

Our research faces a more difficult challenge by reconstructing from feature vectors that do not explicitly aim to keep the person’s identity. A typical face embedding is made up of 512 or more elements [30], the attribute vectors that we are reconstructing from contain 40 and 32 items, describing abstract attributes. A large part of the information from the input image is not required to solve the given task, and should therefore, in theory, have been discarded in early layers of the network - giving reason for the intuitive assumption that they are "safe". We are not the first to implement a reconstruction from such attribute vectors. In 2015, 2016, and 2018, respectively, [21], [11] and [23] published results on the reconstruction of images from different feature representations, like HOG and SIFT descriptors, and the feature maps of a (very small) CNN. All assume full access to the training dataset, and put their focus on understanding network properties, rather than attacking it. [21] iteratively optimize an input image, using gradient descent through the target to minimize a combination of encoder loss and a custom *image prior* term. An image prior can be as simple as the norm of the mean-subtracted image, encouraging the image to stay within a target interval. Their method represents a very early stage of what evolved into

<sup>2</sup> For example Microsoft (<https://learn.microsoft.com/en-us/windows-hardware/design/device-experiences/windows-hello-enhanced-sign-in-security> in September 2023) and Apple (<https://support.apple.com/en-us/102381> in September 2023).

the utilization of image generators: implement additional knowledge about the overall nature of our target images into the loss.

[11] train a decoder with an inverted dataset: for a set of input images of the same type as the target image set (e.g. facial images), the feature vectors that  $E$  returns are determined, and these returned feature vectors then serve as input to  $D$ . The images define the optimal output of  $D$ . The authors follow up with an improved loss function shortly after [10], based on the image- and feature map difference, supplemented by the output of a (very simplistic) discriminator, that is trained alongside the decoder to create more realistic images. The (at the time) innovative use of discriminators makes the images much less blurry.

The same inverted dataset strategy (with no discriminator loss term) achieves better results with an improved decoder architecture in 2019 [40]. In a similar method [43] make use of additional model explanations as a second input to their decoder to improve the accuracy of their reconstruction.

## 2 Threat Model

As depicted in Figure 1, our attack aims at an encoder  $E$  that takes as input an image (in our case a portrait of a person) and returns an output  $f$  describing certain properties of the input image (e.g. an assessment of the emotion of a patient). The vector  $f$  is considered safe, and shared (for example with the intent of scientific evaluation), without (intentionally) linking it to a specific person.

An attacker gains access to  $f$ , has blackbox knowledge about  $E$ , and uses additional assumptions about the kind of input image (facial portraits) to find the identity of the depicted person. It would allow them to leak exceedingly private personal information about their victim.

Generally, our scenario involves three datasets: one used to train  $E$ , one used by the attacker to train  $D$ , and data used at inference time, that was neither seen by  $E$  nor  $D$ . We consider two possibilities for the access to those datasets: **(A)**, the target encoder is trained on images from a public dataset. Then this public dataset can also be used to train  $D$ , and the challenge is to reconstruct images that were never seen by either  $D$  or  $E$ ; and **(B)**, the target is trained on a private dataset. The attacker has no access to this dataset and has to use a more or less good substitute, which makes the task much more challenging.

## 3 Proposed Method

Our method is built around the idea of training a small mapping network to translate a feature vector into a generator input, whereas the strength of the mapping network does not come from its architecture, but rather the training strategy. The exploration of different training methods for that mapping network indicates that *image-based training* (Section 3.2) is a good choice for our context. This training method can be expanded by not only comparing the images directly but also comparing an embedding that is explicitly extracting features that are



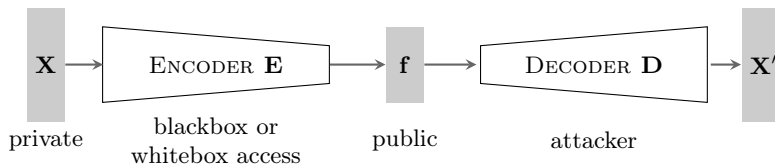


Fig. 1: The scenario of this paper: an encoder  $E$  creates an attribute vector  $f$  for an image, which is reconstructed by our decoder  $D$ .

relevant for our reconstruction goal (Section 3.3). To ultimately combine the results of separate mapping networks trained for specialized loss functions, we propose to make use of the style mixing abilities of a StyleGAN (Section 3.4).

### 3.1 Leveraging image generators to limit the search space

The task of reconstructing an image from a low-dimensional feature vector is fundamentally ill-posed. [16] have shown that adding an imperceptibly small vector to an image can change the created feature vector significantly - two images that are visually the same create different outputs. Vice versa, a single feature vector could have been created by different images. For example, an image that seems like random noise to the human eye can lead to the same output as an actual image.

While we are unable to enforce a bijective relation between image and feature vector, the challenge can be significantly simplified by making sure that our reconstructed images are from a similar distribution as the images that the target encoder has been trained on. If we can define a set of constraints that all reconstructed images should adhere to (e.g. “facial portraits”), we can greatly limit the search space. To infuse that knowledge into the reconstruction pipeline, our approach is based on two steps: (1) train an image generator to create images that satisfy the known limitations and (2) freeze the generator and train a second network to search over the input space of our trained generator. Since a well-trained generator introduces a very strong bias towards a specific type of image, we are adding the same kind of bias to our reconstruction task.

### 3.2 PGE-Training

Our decoder is now made up of two components:  $G$ , a pretrained StyleGAN, and  $P$ , a pre-layer that maps a feature vector to a generator input. Figure 2 illustrates the relation between the three networks involved in the reconstruction. Note that we are only actively training  $P$ , both  $G$  and  $E$  remain frozen, and  $E$  can only be accessed as a blackbox.

The canonical way of training  $P$  would be *noise based training*: generate random noise vectors  $n$  drawn from a Gaussian distribution, feed  $n$  into  $G$ , then  $E$ , and determine the  $f$  that corresponds to  $n$  and minimize the squared distance

between both. A significant advantage would be that we can generate an infinite number of samples, and iterate very quickly through large amounts of training data since the training only involves calculating the gradient for the very small network  $P$ . However, the distribution modeled by  $G$  will likely deviate from the specific distribution of  $X$ . In addition, even the very advanced StyleGAN2 sometimes generates images that are not realistic faces. Therefore, we use what we call *image based training*, which ensures that real face images are used and allows us to control the training data distribution:

1. Select a dataset that is as close as possible to the target dataset<sup>3</sup>,
2. For each image  $X$  in the dataset, retrieve the matching feature vector  $f$  returned by  $E$ , to create a new dataset  $f \rightarrow X$ ,
3. Train  $P$  on this dataset. To evaluate its output  $n$ , it needs to be mapped into the image space, using  $G$ , with the loss defined as  $L(X, G(P(f)))$  for a distance measure  $L$ .

The strategy comes with the obvious disadvantage that even though  $G$  remains frozen, the gradient needs to be propagated through  $G$ , making the training slower. We are also once again limited to the number of samples of our training dataset. Additionally,  $P$  is no longer encouraged to create  $n$  according to Gaussian noise. This difficulty can be largely remedied by adding a term to the overall loss function which we call *distribution loss*:

$$L_{\text{dist}}(n) = \frac{1}{|n|} \sum_{n_i \in n} n_i + |1 - \sigma(n)|, \quad (1)$$

which at least encourages distributions of  $n$  with zero mean and standard deviation  $\sigma = 1$ .

The drawbacks of image-based training are nevertheless outweighed by its advantages: the training is bound to a specific dataset - if  $G$  generates unrealistic images, they are punished by the loss function that compares the output of  $G$  to images from our training set, discouraging any  $n$  that would make  $G$  create such an image while pushing for  $n$  that can reflect the full diversity of the training set. We are further directly comparing images instead of noise, allowing for the advanced loss function presented in Section 3.3.

Note, that we are not using the StyleGAN generator trained with the original method from [20], but a version that is architecturally the same, but trained slightly differently as proposed in [42]. The training leads to generators which are more robust to input that does not perfectly adhere to a Gaussian distribution.

### 3.3 Image Similarity Loss

The basic loss function for the image-based training (Section 3.2) simply compares the pixels of the original and the recreated image. For  $n = P(f)$ , obtained for the feature vector  $f = E(X)$ , the pixel-wise loss  $L_{\text{pixel}}$  is given by

$$L_{\text{pixel}}(n) = (X - G(n))^2 \quad (2)$$

---

<sup>3</sup> In our experiments, this is always the same dataset that  $G$  was trained on

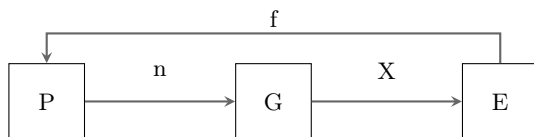


Fig. 2: The in- and outputs of the three components of the reconstruction task: the encoder  $E$  translates an image  $X$  into a feature vector  $f$ , the pre-generator  $P$  creates a generator input from the feature vector, and the generator  $G$  turns the input into an image. The combination of  $P$  and  $G$  makes up the decoder. As described in Section 3.2, our training method is based on keeping  $G$  frozen, but nonetheless comparing not  $n$ , but  $X$  to a defined target.

where  $G$  is the image of the pretrained image generator (see Figure 2).

However, the goal of our attack is not to recreate every pixel but to identify the person seen in the image. Our training needs to focus on the information of the image that is relevant for a human to identify the depicted person, which is not easily defined. A reconstruction of a face that is taken from a different angle could still be identifiable. Contrarily, if a reconstruction gets the exact pixel values of 95% of the target image perfectly right, but fails for a few small, but significant areas, like the shape of the eyes, the depicted person could be unrecognizable. To train explicitly for our defined goal, we are instead comparing the embedding created by the FaceNet [30] network. Both target image and recreation are given to the embedding network, and the loss is given by the squared distance between them:

$$L_{\text{fn}}(n) = (F(X) - F(G(n)))^2. \quad (3)$$

If the embedding created for the target and reconstruction is similar, we can assume that the depicted people have similar identities. Other components of the image, like the pose or the background, are largely disregarded<sup>4</sup>. Less relevance is also given to the coloring of the image, including the color of hair and skin. Both depend on lighting conditions - the same person can appear to have a different hair color in a different image. Invariance to color is a desired property in the context of face recognition.

In contrast, for our reconstruction color of hair and skin is an important aspect. Thus, a good starting point for the FaceNet loss training is a  $P$  that has previously been trained to minimize the pixel-wise error - the pixel-wise error does not truly motivate similar facial features, but steers the overall image towards the right color composition.

<sup>4</sup> We found that even though FaceNet [30] is trained to ignore everything but the identity of the depicted person, images can end up recreating some parts of the pose or background even when trained with nothing but FaceNet embedding loss. This is in line with our main premise: additional information can leak into even very specialized networks.

In total, for a target image  $X$  and its corresponding output  $n$  from  $P$ , our loss is given by

$$L(n) = \lambda_p \cdot L_{\text{pixel}}(n) + \lambda_f \cdot L_{\text{fn}}(n) + \lambda_d \cdot L_{\text{dist}}(n). \quad (4)$$

The distribution term is always weighted with a fixed  $\lambda_d = 0.01$ . Our training starts with pure pixel-wise loss ( $\lambda_p = 1, \lambda_f = 0$ ) until the images no longer improve - we denote the resulting model  $P$  as  $L_{\text{pixel}}$ -model. Then the training is switched to facenet loss ( $\lambda_p = 0, \lambda_f = 1$ ), continuing from the  $L_{\text{pixel}}$ -model, to compute the  $L_{\text{fn}}$ -model.

### 3.4 Using the Layers of a StyleGAN

A StyleGAN differs from other GANs by its *progressive* training method. Each network block is trained progressively for a different image resolution - starting at rough outlines in  $4 \times 4$  images and ending with fine details created by the final block for the highest resolution. The strategy is meant to alleviate the drawback of convolutions and allow a convolutional neural network to model image-wide relations. By starting from tiny images, small enough to be covered by one convolutional kernel, global relations are (said to be) embedded into the lowest layers of the generator.

The training strategy is the reason for a very interesting property of a StyleGAN: each block defines different features of an image, features that can even be distinguished from a human perspective. In our examples, we are using a StyleGAN trained to create  $256 \times 256$  images, whose architecture can be separated into seven blocks. Visible in the example in Figure 3, its first block defines the pose of the depicted person, the second and third different facial features, and the fourth the background. Deeper layers are creating smaller details of the image.



Fig. 3: Stylemixing with a StyleGAN2, between an image  $A$  (leftmost image) and an image  $B$  (rightmost image). For each of the seven images between  $A$  and  $B$ , all generator inputs are the same as for image  $A$ , with the exception of a single vector that was taken from image  $B$ . For the  $i$ -th of those seven images, we replaced the  $i$ -th input vector with the  $B$  vector.

This allows to combine the  $L_{\text{pixel}}$ -model and the  $L_{\text{fn}}$ -model more robustly. We feed the output of  $P$  trained for  $L_{\text{fn}}$  to the second and third block, and

the output of  $P$  trained for only  $L_{\text{pixel}}$  to the rest<sup>5</sup>, deliberately assigning  $P$ s optimized for different loss functions to different aspects of the image.

## 4 Experiments and Results

As the target for our attack, we train a ResNet18 [18] for 300 epochs, minimizing the mean squared distance between the model output and a target attribute vector. The output vectors are made up of 40 or less values, describing abstract properties of both face and image. There are only few publications with the same scenario as our attack, making the most direct competitor the method implemented by [40]. The result of their strategy for our setting is presented in the last row in Figure 5 and 4. Code to recreate our results is available at <https://github.com/ka-anderson/pge-reconstruction>.

To compare our strategies quantitatively, we are assessing the squared distance (MSE) between images and feature vectors, in addition to the structural similarity index measure (SSIM) [36] between images and the similarity between face embedding extracted by VGG-Face [25] and OpenFace [1], face embedding networks similar to FaceNet that were not a part of our reconstruction training. Inspired by [33], we also calculate the distance scores between two distinct subsets of CelebA as a baseline, to find that if the images are from the same distribution, but otherwise completely different, the differences are at MSE 0.62, SSIM 0.06, VGG-Face 0.0005 and OpenFace 0.0037.

To the best of our knowledge, there is currently no perfect metric for the visual similarity of two portraits. A standard facial embedding disregards details, like the coloring of the image, while a measure created for the overall similarity of images weights all image areas equally. Additionally, while the statistics are useful to compare images from the same distribution, all are likely to be "fooled" by images from unexpected distributions, like the relatively blurry images from [40]. To compare our images to the previous state-of-the-art, we are instead evaluating the results of a designated user study (see Figure 2): 19 participants are asked to determine the most likely original for a reconstruction, given a selection of five portraits that would have resulted in a similar attribute vector.

### 4.1 D and E trained on the same dataset

In the scenario of an attack on an encoder that was trained on a public dataset, our  $E$  is trained to extract a 32-element attribute vector. The vector describes basic image and facial properties (like emotion, hair and image brightness), in addition to the position and angle of the depicted face<sup>6</sup>. Both  $E$  and  $D$  (i.e. the frozen image generator  $G$  and the pregenerator  $P$ ) are trained on FFHQ. To evaluate the attack, we are feeding new images from CelebA to  $E$  and then applying our trained reconstruction networks to recreate the original image from

<sup>5</sup> Both  $L_{\text{fn}}$  and  $L_{\text{pixel}}$  are always used in combination with  $0.01 \cdot L_{\text{dist}}$

<sup>6</sup> The features are extracted from <https://github.com/DCGM/ffhq-features-dataset>

the feature vector. Figure 4 presents a qualitative evaluation of nine randomly selected images.

Even though the FaceNet loss started from images that were approximately correct in terms of skin and hair color, the reconstruction is sometimes shifted towards a different coloring over time. The difference becomes especially evident from the fact that the FFHQ dataset exhibits some degree of diversity in terms of skin color, which CelebA is lacking entirely - while all nine random CelebA images are taken from subjects with light skin, some of the FaceNet reconstructions are different. The stylemixing fusion strategy helps to maintain the overall coloring scheme extracted by the pixel loss, combining them with the more detailed facial features extracted by the embedding loss. Looking at the recreation for the last random target image (last column) reveals that there is a small chance that our process fails entirely, maybe caused by an erroneous feature vector, maybe by an unusual combination of attributes.

The results by [40] are also recreating basic attributes, however, all reconstructed images are blurry and visually close to the same "average face". While their images usually represent attributes like age and pose correctly, additional information like the shape of the eyes, face and mouth, is barely distinguishable in their images. The images created by our predecessor do come with one advantage: because the images are not bound to the distribution of actual human faces, the scores for common image evaluation methods are quite high, indicating that they could be more useful when attempting to fool a facial recognition software (MSE 0.078, SSIM 0.403, VGG-Face 0.00015, OpenFace 0.0047). Seen in Figure 2, both strategies achieve a maximum user recognition rate of 80%. In terms of average recognition rate and number of false answers ("subtract false answers"), our method outperforms the predecessor.

The metrics shown in Table 1 are in line with our qualitative evaluation: the pixel loss minimizes the difference between images pixels (visible in both mean squared distance and SSIM), while the FaceNet loss minimizes the loss between facial embeddings, though sacrificing pixel accuracy. The combination of both results in almost the same pixel distance as pure pixel based loss training, but with a lower embedding distance. Notable is that the stylemixing significantly decreases the distance between feature vectors - the images are most similar from the perspective of the encoder.

Interestingly, even though hair color is not included in the attribute vector, the reconstruction manages to distinguish "brown" and "not brown" hair with surprising reliability.

## 4.2 D and E trained on different datasets

For the second setting, we evaluate our attack against an encoder that was trained to extract a 40-element binary attribute vector on CelebA, while our decoder is still trained on FFHQ. Note that the attribute vectors of this experiment include no information about the position or angle of the depicted face. The reconstruction is evaluated on a subset of CelebA that was never seen by

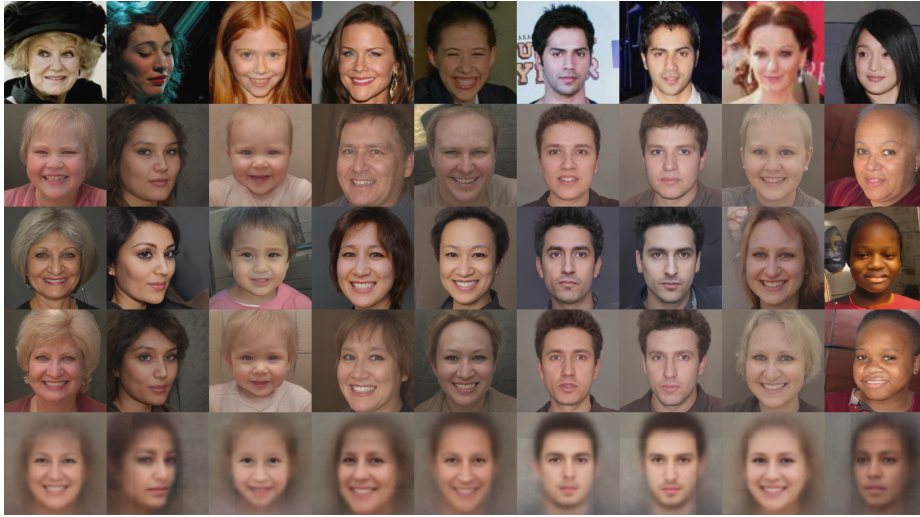


Fig. 4: Reconstructions for random images of the CelebA dataset, for a  $D$  and  $E$  both trained on FFHQ. From top to bottom, the rows present the target images, the result of the pixel-wise loss, the FaceNet embedding loss, and the fused version of the two. The final row displays the outcome of our predecessor, [40]. Details about training can be found in Section 4.1.

$E$ . Hence,  $D$  is not only trained on different images than  $E$  but even on images drawn from a different distribution.

It is clear from both the quantitative evaluation of randomly selected example images (Figure 5) and the calculated statistics (Table 1 and Figure 2) that this task is more difficult. However, while the pixelwise loss is sometimes unable to create a similar image, the FaceNet loss usually helps the model project matching facial features onto the sometimes otherwise mismatched portraits, proving that this loss formulation is more stable to the challenge of diverging datasets.

The attribute vector used for this reconstruction setting does not include information about the pose of the depicted person. Interestingly, for the images taken from the side, the recreated person is photographed from a similar angle.

This information, e.g., is not extracted by [40]: all images are from a frontal perspective, and all are slight variations of an average human portrait, providing much less information about exact facial features than our reconstruction. But, like for the previous setting, scores like MSE and SSIM are higher - possibly because using the "average" for many pixels allows to minimize the loss, despite the absence of distinguishing features (MSE 0.075, SSIM 0.426, VGG-Face 0.00014, OpenFace 0.0050).



Fig. 5: Reconstructions for random images of the CelebA test set, for a  $D$  trained on FFHQ and  $E$  trained on the CelebA training set. From top to bottom, the rows present the target images, the result of the pixelwise loss, the FaceNet embedding loss, the fused version of the two and the results from [40]. Details about training can be found in Section 4.2.

## 5 Conclusion

This work introduced a novel reconstruction pipeline, operating with only a low-dimensional vector representing high-level attributes of a portrait and black-box access to the encoder network. The reconstruction surpassed the perceptual quality of previous work in this setting by leveraging recent advances in image generation and facial identification. A pivotal step involved merging the model trained on face embedding loss for mere individual identity with the model from pixel loss for finer image details. This integration was achieved by directing their outputs into distinct layers of the StyleGAN.

Our results show that already a low-dimensional attribute vector and only black-box access to the encoder network can allow unexpected conclusions about the original image - most notable the identity of the depicted person. In a user study we observed recognition rates up to 79%. But also additional details like the angle from which the portrait was taken can be extracted. Despite being intended to encode nothing but a small number of abstract features, the target network inadvertently captures more information from its input than just those features. It’s crucial to recognize that a neural network, when employed conventionally, can convey much more information from a high-dimensional input to a low-dimensional output than expected. Consequently, the output of a neural network must be treated with the same level of care as the input.



Table 1: Quantitative evaluation of our reconstruction of CelebA test images for  $D$  trained on FFHQ, and  $E$  on FFHQ (top) and the CelebA training set (bottom).

		MSE		SSIM	VGG-Face	OpenFace
		X	f			
FFHQ	$L_{\text{pixel}}$	0.3535	7.8280	0.1200	0.0003272	0.004061
	$L_{\text{fn}}$	0.4017	4.5761	0.1247	0.0003367	0.003797
	mixed	0.3417	3.3914	0.1302	0.0003138	0.003723
CelebA	$L_{\text{pixel}}$	0.4387	0.2059	0.0934	0.0003947	0.003992
	$L_{\text{fn}}$	0.4399	0.1759	0.1016	0.0003631	0.003934
	mixed	0.4302	0.1744	0.0972	0.0003967	0.004053

Table 2: Results of a user study for the two scenarios (see Section 4.1 for the "FFHQ" 4.2 for "CelebA"), by our method and [40]. The score for an image is determined by the number of correct answers. In the second column, we are counting a correct answer as one, no answer as zero, and a false answer as minus one.

		% correct answers		% correct - % incorrect	
		best image	mean	best image	mean
FFHQ	ours	79	42	79	15
	Yang	79	29	73	-22
CelebA	ours	68	36	63	11
	Yang	53	39	16	5

## References

- Baltrušaitis, T., Robinson, P., Morency, L.P.: Openface: An open source facial behavior analysis toolkit. In: 2016 IEEE Winter Conference on Applications of Computer Vision (WACV) (2016)
- Bertran, M., Martinez, N., Papadaki, A., Qiu, Q., Rodrigues, M., Reeves, G., Sapiro, G.: Adversarially learned representations for information obfuscation and inference. In: ICLR (2019)
- Bosch, N., D’Mello, S.K., Baker, R.S., Ocumpaugh, J., Shute, V., Ventura, M., Wang, L., Zhao, W.: Detecting student emotions in computer-enabled classrooms. In: Proceedings of the Twenty-Fifth International Joint Conference on Artificial Intelligence (2016)
- Chen, S., Kahla, M., Jia, R., Qi, G.J.: Knowledge-enriched distributional model inversion attacks. ICCV pp. 16158–16167 (2020)
- Deng, J., Guo, J., Xue, N., Zafeiriou, S.: Arcface: Additive angular margin loss for deep face recognition. In: CVPR (2019)
- Ding, X., Fang, H., Zhang, Z., Choo, K.K.R., Jin, H.: Privacy-preserving feature extraction via adversarial training. IEEE Transactions on Knowledge and Data Engineering pp. 1967–1979 (2020)

7. Dionysiou, A., Vassiliades, V., Athanasopoulos, E.: Exploring model inversion attacks in the black-box setting. *Proceedings on Privacy Enhancing Technologies* pp. 190–206 (2023)
8. Dong, X., Jin, Z., Guo, Z., Jin Teoh, A.B.: Towards generating high definition face images from deep templates. In: *BIOSIG*. pp. 1–11 (2021)
9. Dong, X., Miao, Z., Ma, L., Shen, J., Jin, Z., Guo, Z., Teoh, A.B.J.: Reconstruct face from features based on genetic algorithm using gan generator as a distribution constraint. *Computers and Security* (2023)
10. Dosovitskiy, A., Brox, T.: Generating images with perceptual similarity metrics based on deep networks. In: Lee, D., Sugiyama, M., Luxburg, U., Guyon, I., Garnett, R. (eds.) *Advances in Neural Information Processing Systems* (2016)
11. Dosovitskiy, A., Brox, T.: Inverting visual representations with convolutional networks. In: *CVPR* (2016)
12. Duong, C.N., Truong, T.D., Luu, K., Quach, K.G., Bui, H., Roy, K.: Vec2face: Unveil human faces from their blackbox features in face recognition. In: *CVPR*. pp. 6132–6141 (2020)
13. Esteve, A., Kuprel, B., Novoa, R.A., Ko, J., Swetter, S.M., Blau, H.M., Thrun, S.: Dermatologist-level classification of skin cancer with deep neural networks. *nature* **542**(7639) (2017)
14. Fredrikson, M., Jha, S., Ristenpart, T.: Model inversion attacks that exploit confidence information and basic countermeasures. In: *ACM SIGSAC Conference on Computer and Communications Security (CCS)*. p. 1322–1333 (2015)
15. Gao, H., Yüce, A., Thiran, J.P.: Detecting emotional stress from facial expressions for driving safety. In: *ICIP* (2014)
16. Goodfellow, I., Shlens, J., Szegedy, C.: Explaining and harnessing adversarial examples. In: *ICLR* (2015)
17. Han, G., Choi, J., Lee, H., Kim, J.: Reinforcement learning-based black-box model inversion attacks. In: *CVPR*. pp. 20504–20513 (2023)
18. He, K., Zhang, X., Ren, S., Sun, J.: Deep residual learning for image recognition. In: *CVPR*. pp. 770–778 (2016)
19. Kahla, M., Chen, S., Just, H.A., Jia, R.: Label-only model inversion attacks via boundary repulsion. *CVPR* pp. 15025–15033 (2022)
20. Karras, T., Laine, S., Aittala, M., Hellsten, J., Lehtinen, J., Aila, T.: Analyzing and improving the image quality of stylegan. In: *CVPR*. pp. 8110–8119 (2020)
21. Mahendran, A., Vedaldi, A.: Understanding deep image representations by inverting them. In: *CVPR* (2015)
22. Mai, G., Cao, K., Yuen, P.C., Jain, A.K.: On the reconstruction of face images from deep face templates. *IEEE Transactions on Pattern Analysis and Machine Intelligence* pp. 1188–1202 (2019)
23. Nash, C., Kushman, N., Williams, C.K.I.: Inverting supervised representations with autoregressive neural density models. In: *International Conference on Artificial Intelligence and Statistics* (2018)
24. Osia, S.A., Taheri, A., Shamsabadi, A.S., Katevas, K., Haddadi, H., Rabiee, H.R.: Deep private-feature extraction. *IEEE Transactions on Knowledge and Data Engineering* pp. 54–66 (2018)
25. Parkhi, O.M., Vedaldi, A., Zisserman, A.: Deep face recognition. In: *British Machine Vision Conference* (2015)
26. Pittaluga, F., Koppal, S., Chakrabarti, A.: Learning privacy preserving encodings through adversarial training. In: *2019 IEEE Winter Conference on Applications of Computer Vision (WACV)*. pp. 791–799. *IEEE* (2019)

27. Raval, N., Machanavajjhala, A., Cox, L.P.: Protecting visual secrets using adversarial nets. In: CVPR Workshops. pp. 1329–1332 (2017)
28. Ren, Z., Lee, Y.J., Ryoo, M.S.: Learning to anonymize faces for privacy preserving action detection. In: ECCV. pp. 620–636 (2018)
29. Roy, P.C., Boddeti, V.N.: Mitigating information leakage in image representations: A maximum entropy approach. In: CVPR. pp. 2586–2594 (2019)
30. Schroff, F., Kalenichenko, D., Philbin, J.: Facenet: A unified embedding for face recognition and clustering. In: CVPR. pp. 815–823 (2015)
31. Shahreza, H.O., Hahn, V.K., Marcel, S.: Face reconstruction from deep facial embeddings using a convolutional neural network. In: ICIP. pp. 1211–1215 (2022)
32. Simonyan, K., Vedaldi, A., Zisserman, A.: Deep inside convolutional networks: Visualising image classification models and saliency maps. In: ICLR Workshops (2014)
33. Tinsley, P., Czajka, A., Flynn, P.: This face does not exist... but it might be yours! identity leakage in generative models. pp. 1319–1327
34. Vendrow, E., Vendrow, J.: Realistic face reconstruction from deep embeddings. In: NeurIPS 2021 Workshop Privacy in Machine Learning (2021)
35. Wang, J., Zhang, J., Bao, W., Zhu, X., Cao, B., Yu, P.S.: Not just privacy: Improving performance of private deep learning in mobile cloud. In: ACM SIGKDD international conference on knowledge discovery & data mining. pp. 2407–2416 (2018)
36. Wang, Z., Bovik, A.C., Sheikh, H.R., Simoncelli, E.P.: Image quality assessment: From error visibility to structural similarity. *Trans. Img. Proc.* p. 600–612 (2004)
37. Whitehill, J., Serpell, Z., Lin, Y.C., Foster, A., Movellan, J.R.: The faces of engagement: Automatic recognition of student engagement from facial expressions. *IEEE Transactions on Affective Computing* (2014)
38. Wu, Z., Wang, H., Wang, Z., Jin, H., Wang, Z.: Privacy-preserving deep action recognition: An adversarial learning framework and a new dataset. *IEEE Transactions on Pattern Analysis and Machine Intelligence* pp. 2126–2139 (2020)
39. Wu, Z., Wang, Z., Wang, Z., Jin, H.: Towards privacy-preserving visual recognition via adversarial training: A pilot study. In: ECCV. pp. 606–624 (2018)
40. Yang, Z., Zhang, J., Chang, E.C., Liang, Z.: Neural network inversion in adversarial setting via background knowledge alignment. In: ACM SIGSAC Conference on Computer and Communications Security. pp. 225–240 (2019)
41. Zhang, Y., Jia, R., Pei, H., Wang, W., Li, B., Song, D.X.: The secret revealer: Generative model-inversion attacks against deep neural networks. *CVPR* pp. 250–258 (2019)
42. Zhao, S., Liu, Z., Lin, J., Zhu, J.Y., Han, S.: Differentiable augmentation for data-efficient gan training. *Advances in neural information processing systems* **33**, 7559–7570 (2020)
43. Zhao, X., Zhang, W., Xiao, X., Lim, B.Y.: Exploiting explanations for model inversion attacks. *ICCV* pp. 662–672 (2021)